Modal frequency degeneracy in thermally loaded optical resonators

Amber L. Bullington,* Brian T. Lantz, Martin M. Fejer, and Robert L. Byer

E. L. Ginzton Laboratory, Stanford University, Stanford, California, USA

*Corresponding author: abull@stanford.edu

Received 4 December 2007; revised 11 April 2008; accepted 18 April 2008;
posted 21 April 2008 (Doc. ID 90278); published 14 May 2008

We observe power coupling from the fundamental mode to frequency-degenerate higher-order spatial modes in optical resonators illuminated with a 30 W laser. Thermally-induced modal frequency degeneracy facilitates power transfer from the fundamental mode to higher-order modes, reduces power coupling into the cavity, and triggers power fluctuations. Modeling thermoelastic deformation of a mirror's surface shows predicted modal frequency degeneracy to be in reasonable agreement with experimental observations. Predictions for the Laser Interferometer Gravitational-wave Observatory (LIGO) show that the circulating fundamental-mode power necessary for gravitational-wave detection is compromised at coating absorptions of 3.8 and 0.44 ppm for Enhanced and Advanced LIGO Fabry–Pérot cavities, respectively. © 2008 Optical Society of America

OCIS codes: 140.0140, 140.4780, 140.6810, 230.5750, 260.5740.

1. Introduction

Degradation of laser beam quality from coupling to frequency-degenerate higher-order modes is a serious concern when diffraction-limited, fundamental-mode power enhancement in an optical resonator is desired. Frequency degeneracy of higher-order modes has been reported in solid-state lasers from thermal effects [1,2] and in optical resonators from small-angle scattering [3]. The high circulating power required for gravitational-wave detectors including LIGO, the Laser Interferometer Gravitational-wave Observatory, makes understanding thermally-induced modal frequency degeneracy critical for interferometer performance. We explore and model accidental frequency degeneracy of higher-order modes with the fundamental mode, showing power limitations to interferometer performance in the context of LIGO. However, the results apply to any resonant laser system requiring high-power and fundamental-mode operation.

LIGO's sensitivity for gravitational-wave detection is limited by shot noise above 250 Hz [4], making increased laser power desirable for detecting gravitational-wave signals above this frequency. The planned upgrade to LIGO, known as Advanced LIGO, calls for a twentyfold increase in incident laser power to 200 W compared to LIGO's current 10 W laser [4]. An interim upgrade to the detector, Enhanced LIGO, utilizes an increase in laser power to 35 W [5]. Thermally-induced distortion of interferometer optics from thermal lensing and thermoelastic deformation limit improvements to detector sensitivity [6]. While thermal lensing can significantly impact the beam coupled into and out of a stable optical resonator, thermoelastic deformation alters the eigenmodes of a cavity, leading to accidental frequency degeneracy and power coupling between the fundamental mode and higher-order modes. We focus on thermoelastic deformation that induces accidental frequency degeneracy and its consequences for LIGO.

In LIGO, the highest thermoelastic deformation occurs in Fabry–Pérot cavities in the arms of the Michelson interferometer and in the ring resonators, known as modecleaners, that provide input-beam spatial and spectral filtering. Absorption in highly reflecting dielectric coatings dominates the thermo-

0003-6935/08/152840-12$15.00/0

elastic deformation in these cavities. While coating absorption of 1 ppm or less is achievable with current coating technology, thermal effects remain a concern for future LIGO interferometers. For example, the circulating power in the Advanced LIGO arm cavities is proposed to reach 800 kW, making coatings with absorption of less than 1 ppm a necessity to avoid accidental modal frequency degeneracy.

We study the effects of thermal loading with available laser power using a specially designed modecleaner with calibrated absorption loss. Figure 1 shows a schematic of the table-top modecleaner used in the experiment. It consists of mirrors attached to a fused silica spacer with drilled openings for the circulating beam to traverse free space. The curved mirror is attached to a piezo-electric transducer (PZT) for adjusting the cavity length. A calibrated absorption loss is achieved by using an infrared-absorbing glass for the substrate of the curved mirror, M_3. Light at the 1064 nm operating wavelength leaks through the dielectric coating of M_3 and is absorbed in a thin layer of the substrate beneath the coating. All mirrors have dielectric coatings with absorption loss not exceeding 1 ppm as measured with photothermal common-path interferometry [7]. For this experiment, a low-loss coating on a highly absorbing substrate gives a more effective calibrated absorption loss than a weakly absorbing coating because of better uniformity and known linear absorption in the substrate [8].

A spatially filtered 30 W laser illuminates two modecleaners with different absorption loss. The curved mirror of the "absorbing modecleaner" is made of an infrared-absorbing glass. The "low-loss modecleaner" utilizes low-loss BK-7 glass substrates for all of its mirrors. M_1 and M_2 of the absorbing modecleaner are fused silica optics with low-loss coatings. Low-loss substrates for M_1 and M_2 avoid thermal focusing of the input and output beams.

We begin by presenting a model for accidental frequency degeneracy induced by thermoelastic deformation of a resonator mirror from laser heating. We then present experimental results demonstrating accidental frequency degeneracy, followed by predictions for the thermal performance of future LIGO detectors.

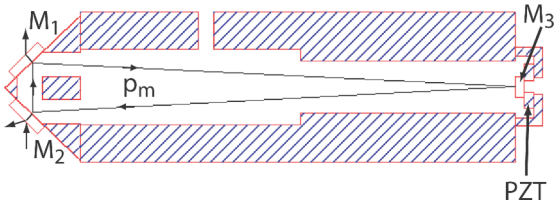

Fig. 1. (Color online) Schematic of a ring resonator (modecleaner). M_1 and M_2 are 1 in. in diameter, and M_3, attached to a piezo-electric transducer (PZT), is 0.5 in. in diameter with a 1 m radius of curvature. Round-trip perimeter, p_m, is 42 cm.

2. Modeling of Modal Frequency Degeneracy Induced by Mirror Thermoelastic Deformation

In this section we present a model for accidental frequency degeneracy caused by thermoelastic deformation due to power absorbed in a mirror from an incident Gaussian laser beam. We start by introducing resonator field equations, resonant frequency conditions for a modecleaner, and impedance matching that determine the thermal load seen by the resonator mirrors. The resulting thermoelastic deformation induces changes in the mirror curvature that leads to changes in a resonator's characteristics, namely eigenmode waist size and cavity g-factor product, $g_1 g_2$. As a consequence, higher-order modal resonance frequencies shift as a function of absorbed power and accidental frequency degeneracies occur with the fundamental mode. The thermally-induced distortion allows power to couple from the fundamental mode to frequency-degenerate higher-order modes, resulting in power loss of the circulating fundamental mode.

A. Resonator Electric Fields, Modecleaner Resonant Modal Frequencies and Impedance Matching

From Siegman [9], the intracavity circulating field, E_{circ}, and reflected field, E_{refl}, for a modecleaner are related to the input field, E_{in}, by

$$\frac{E_{\mathrm{circ}}}{E_{\mathrm{in}}} = \frac{j\sqrt{T_1}}{1-\sqrt{R_1R_2R_3}\exp(-l_{RT}/2 - j\omega p_m/c)}, \quad (1a)$$

$$\frac{E_{\mathrm{refl}}}{E_{\mathrm{in}}} = \frac{\sqrt{R_1}-\sqrt{R_2R_3}\exp(-l_{RT}/2 - j\omega p_m/c)}{1-\sqrt{R_1R_2R_3}\exp(-l_{RT}/2 - j\omega p_m/c)}, \quad (1b)$$

where R_1, R_2, and R_3 are the power reflectivities of mirrors M_1, M_2, and M_3, respectively, and T_1 is the power transmissivity of M_1, as shown in Fig. 1. p_m is the round-trip optical path of the ring-resonator modecleaner. ω and c are the frequency and the speed of light, respectively. l_{RT} is the power lost in the modecleaner in one round-trip.

For the thermal loading experiment, cavities are locked to fundamental-mode resonance using the Pound–Drever–Hall technique [10]. The phase condition for resonance is given by

$$\omega p_m/c = 2\pi. \quad (2)$$

An eigenmode resonance frequency, $\omega_{\sigma q}$, satisfies Eq. (2), giving $\omega = \omega_{\sigma q}$. This eigenmode resonance frequency normalized to the axial mode spacing, $\Delta\omega_{ax}$, is written as $\bar{\omega}_{\sigma q} = \omega_{\sigma q}/\Delta\omega_{ax}$ and is given by

$$\bar{\omega}_{\sigma q} = q + \frac{\sigma+1}{\pi}\cos^{-1}[(g_1g_2)^{1/2}], \quad (3)$$

where $\bar{\omega}_{\sigma q}$ is the normalized frequency of the qth axial mode and σ is the mode-index sum [9]. Here g_1

and g_2 are the g-factors of a resonator given by $g = 1 - L/R$. For a Hermite–Gaussian mode represented by TEM_{mn},

$$\sigma_{HG} = m + n, \tag{4}$$

where m and n are the number of nodes in the horizontal and vertical directions, respectively. Similarly for a Laguerre–Gaussian mode represented by LG_{pl},

$$\sigma_{LG} = 2p + l, \tag{5}$$

where the number of radial and azimuthal nodes are given by p and l, respectively. σ can be either σ_{HG} or σ_{LG}, depending on the basis set for a resonant mode. In practice, both Hermite–Gaussian and Laguerre–Gaussian modes can be excited in a stable resonator.

The three-bounce geometry of a modecleaner results in an additional π phase shift for higher-order modes with certain symmetry. This π phase shift resets their resonance frequency by half the axial mode spacing. For TEM_{mn} modes with m odd and LG_{pl} modes with l even and $l > 0$, the modal resonance frequencies are given by

$$\bar{\omega}_{\sigma^* q} = q + \frac{\sigma^* + 1}{\pi}\cos^{-1}[(g_1 g_2)^{1/2}] + \frac{1}{2}, \tag{6}$$

where σ^* indicates the given mode-index sum requires this additional frequency shift. In any resonator with an odd number of reflections, this π phase shift occurs for odd TEM_{mn} and even LG_{pl} eigenmodes regardless of polarization. A resonator with even-numbered reflections, such as a two-bounce or four-bounce cavity, does not have any eigenmodes with shifted resonance frequencies.

For a cavity with high-reflectance mirrors that meets the resonant phase condition of Eq. (3), the denominator of Eqs. (1a) and (1b) can be approximated as

$$1 - \sqrt{R_1 R_2 R_3}\exp(-l_{RT}) \approx 1 - \sqrt{1 - l_{RT}} \approx l_{RT}/2 \tag{7}$$

assuming $\exp(-l_{RT}) \approx (1 - l_{RT})$. From Eqs. (2) and (7), the circulating power, P_{circ}, on resonance simplifies to

$$\frac{P_{\mathrm{circ}}}{P_{\mathrm{in}}} \approx \frac{4T_1}{l_{RT}^2}. \tag{8}$$

Cavity finesse can be written approximately as $2\pi/l_{RT}$ [9], giving a simple relation between circulating power and finesse, F, as

$$\frac{P_{\mathrm{circ}}}{P_{\mathrm{in}}} \approx \frac{2T_1}{\pi l_{RT}}F. \tag{9}$$

Maximum circulating power is achieved when a resonator is impedance matched. The impedance-matching condition is determined by setting the reflected power in Eq. (1a) to zero, implying all incident power is coupled into the cavity. The impedance-matching condition on resonance is given by

$$2T_1 = l_{RT}. \tag{10}$$

For a modecleaner, l_{RT} is written as

$$l_{RT} = T_1 + T_2 + a_c + l_c, \tag{11}$$

where T_2 is the transmission of mirror M_2, a_c is the total coating absorption, and l_c accounts for residual losses from scatter or optic imperfections. For the absorbing modecleaner, the transmission through mirror M_3, known as T_3, is defined to be the total coating absorption loss for the cavity as

$$a_c \equiv T_3, \tag{12}$$

since all power transmitted through M_3 is absorbed. a_c is the sum of the coating absorptions for the low-loss modecleaner. Power absorbed in the cavity is related to P_{circ} via

$$P_{abs} = a_c P_{\mathrm{circ}}. \tag{13}$$

Absorbed power for the absorbing modecleaner is calculated from the measured transmitted power, P_{trans}, to be

$$P_{abs} = \frac{T_3}{T_2}P_{\mathrm{trans}}. \tag{14}$$

For the absorbing modecleaner, $T_2 = 0.008$ and $T_3 = 81$ ppm, giving $T_3/T_2 = 0.01$.

B. Model for Thermoelastic Deformation

Absorption in dielectric coatings, and the resulting thermoelastic deformation of the mirror surfaces, is considered in this section. By assuming the deformation in the vicinity of the beam waist at a mirror's surface is spherical, Winkler, *et al.* [11] approximate the thermoelastic deformation as a change in the depth of curvature or sagitta across the incident Gaussian beam diameter. The change in sagitta, δs, of a mirror is related to absorbed power in its coating via

$$\delta s = \frac{\alpha}{4\pi\kappa}P_{abs}, \tag{15}$$

where α and κ are the thermal expansion coefficient and the thermal conductivity of the optical substrate, respectively [11]. The relation between undistorted (cold) sagitta, s_{cold}, and radius of curvature, R_{cold}, is given by

$$R_{\mathrm{cold}} = \frac{w_{\mathrm{cold}}^2}{2s_{\mathrm{cold}}}, \tag{16}$$

where w_{cold} is the unperturbed fundamental-mode beam radius incident on the mirror.

The ring-resonator modecleaner has a two-mirror equivalent cavity that consists of a flat mirror spaced half the modecleaner's perimeter, $L_m = p_m/2$, from the curved mirror M_3. The flat mirror is positioned at the eigenmode waist of the modecleaner. From Winkler *et al.* [11], the change in beam radius at the flat mirror from distortion of M_3 for a two-mirror resonator is given by

$$\frac{\delta w_{1,M_3}}{w_1} = -\frac{\pi}{2\lambda}\frac{\delta s_3}{[g_1 g_2(1-g_1 g_2)]^{1/2}}, \tag{17}$$

where λ is the wavelength of light, w_1 is the beam radius at M_1, and δs_3 is the sagittal change at M_3. A two-mirror, modecleaner-equivalent cavity has $g_1 = 1$ and $g_2 = 1 - L_m/(R_{\mathrm{cold},M_3})$, where R_{cold,M_3} is the undistorted radius of curvature of M_3.

For the absorbing modecleaner, the small thermoelastic deformation of M_1 and M_2 is much less than the deformation of mirror M_3. Thus, any contribution to the distortion of the eigenmode waist radius from M_1 and M_2 is neglected.

From Eq. (16) the thermally altered, "hot" radius of curvature of a mirror is $R_{\mathrm{hot}} = w_{\mathrm{hot}}^2/(2s_{\mathrm{hot}})$, where the hot beam radius and sagitta are given by

$$w_{\mathrm{hot}} = w_{\mathrm{cold}} - \delta w, \tag{18}$$

$$s_{\mathrm{hot}} = s_{\mathrm{cold}} - \delta s. \tag{19}$$

The minus sign in Eq. (17) results in an increase in beam radius with a corresponding decrease in sagitta. Thus, mirror radius of curvature and cavity g-factor product increase with absorbed power.

C. Degenerate Higher-Order Mode Frequencies

The thermally-induced change in mirror curvature affects the modal frequency spacing of a thermally loaded cavity. Modal frequency spacing changes very little from the thermally-induced change in modecleaner length compared to the change in radius of curvature of the cavity's mirrors [12]. Thus, any change in cavity g-factors may be approximated as a change in radius of curvature alone. For example, the hot g-factor product, $g_1 g_{2,\mathrm{hot}}$, of the equivalent two-mirror absorbing modecleaner is written as ($g_1 = 1$ from Eq. (17))

$$g_1 g_{2,\mathrm{hot}} = 1 - \frac{L_m}{R_{\mathrm{hot},M_3}}. \tag{20}$$

The modal frequency spacing and higher-order modal frequency degeneracies for a thermally loaded cavity are calculated from this hot g-factor product.

Thermoelastic deformation of mirror curvature and the resulting change in $g_1 g_2$ alter the resonance frequencies of all modes supported by a cavity. A higher-order mode can become degenerate with the fundamental mode in frequency when

$$\bar{\omega}_{\sigma q'} - \bar{\omega}_{0q} = \frac{\sigma}{\pi}\cos^{-1}[(g_1 g_{2,\mathrm{hot}})^{1/2}] + (q' - q) = k \tag{21}$$

or

$$\bar{\omega}_{\sigma^* q'} - \bar{\omega}_{0q} = \frac{\sigma^*}{\pi}\cos^{-1}[(g_1 g_{2,\mathrm{hot}})^{1/2}] + \frac{1}{2} + (q' - q) = j, \tag{22}$$

where k and j are integers. The change in modal resonance frequency with respect to $g_1 g_{2,\mathrm{hot}}$ is dependent on the mode-index sum, σ or σ^*.

Figure 2 shows a plot of normalized resonance frequency, $\bar{\omega}_{\sigma q}$, versus $g_1 g_2$ for the TEM_{00} and $\mathrm{TEM}_{11,0}$ modes of a modecleaner. The resonance frequency of $\mathrm{TEM}_{11,0}$ changes considerably compared to the fundamental-mode resonance. (The choice of $\mathrm{TEM}_{11,0}$ will become apparent in Section 3.) The cold-cavity $g_1 g_2$ of a modecleaner is 0.79, as marked by a vertical line on the plot. A higher-order mode overlaps with the fundamental mode in frequency as thermal loading increases the cavity's g-factor product. Figure 2 shows the frequency degeneracy between $\mathrm{TEM}_{11,0}$ and TEM_{00} for $g_1 g_{2,\mathrm{hot}}$ equal to 0.8274.

D. Power Coupling between Modes

Power may couple from the fundamental mode to a frequency-degenerate higher-order mode if the coupling coefficient between them is nonzero. Thermal distortion of resonator mirrors or imperfections such as surface roughness or scatter contribute to nonzero mode coupling. In general, the spatial-mode amplitude coupling coefficient between the fundamental and another mode, c_{00mn}, can be written as

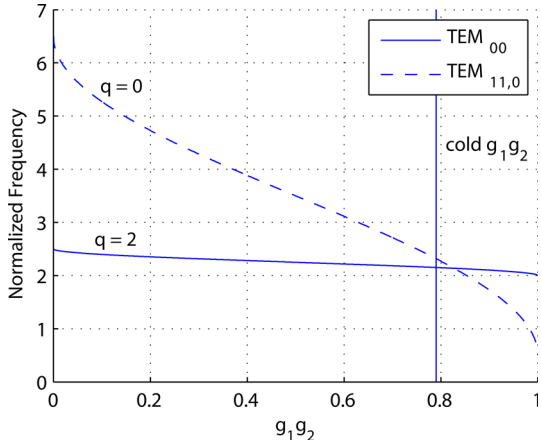

Fig. 2. (Color online) Normalized modal resonance frequency, $\bar{\omega}_{\sigma q}$, versus $g_1 g_2$ for the qth axial $\mathrm{TEM}_{11,0}$ and (qth + 2) TEM_{00} modes of a modecleaner. A vertical line at $g = 0.79$ indicates a modecleaner's undistorted (cold) $g_1 g_2$. The resonance frequency of $\mathrm{TEM}_{11,0}$ changes significantly compared to TEM_{00}, overlapping in resonance with the fundamental mode for $g_1 g_2 = 0.8274$. Since σ is odd for $\mathrm{TEM}_{11,0}$, where $\sigma = m + n$ for a TEM_{mn} mode, this mode's resonance frequency is shifted by half the cavity's axial mode spacing.

$$c_{00mn} = \int u_{00}^{*}(x,y)d(x,y)u_{mn}(x,y)\mathrm{d}A, \tag{23}$$

where u_{00} and u_{mn} are basis functions of the unperturbed resonator [13,14]. $d(x,y)$ is a complex function describing the mirror distortion. From Kogelnik [15], the fraction of power coupled between modes is given by

$$\kappa_{00mn} = |c_{00mn}|^2. \tag{24}$$

Power transfer between the fundamental mode and a higher-order mode becomes appreciable with nonzero spatial-mode coupling and frequency degeneracy between modes. The term "modal frequency degeneracy" describes this thermally-induced resonant coupling phenomenon.

A cavity is "mode-matched" if the incident mode waist and curvature matches the intracavity fundamental mode with no thermal distortion ($d(x,y) = 1$), giving $\kappa_{0000} = 1$. κ_{0000} decreases as resonator mirrors thermally deform from increasing absorbed power. In addition to this spatial mode-matching factor, power coupled to frequency-degenerate higher-order modes also degrades coupling of the incident beam into the resonator. Negligible coupling occurs from the incident beam to an intracavity frequency-degenerate higher-order mode [15]. The round-trip loss from Eq. (11) is written to include input-beam coupling degradation from power coupled to k frequency-degenerate higher-modes as

$$l_{RT} = T_1 + T_2 + a_c + l_c + a_{\mathrm{eff}}, \tag{25}$$

where

$$a_{\mathrm{eff}} = \sum_{i=1}^{k} \kappa_{00mn,i} \tag{26}$$

and $\kappa_{00mn,i}$ is the fraction of power coupled to the ith mode.

Since the transmission through M_3 of the absorbing modecleaner represents an absorption loss as given by Eq. (12), the impedance-matching condition derived from Eq. (27) that ensures the absorbing modecleaner is nearly impedance-matched gives

$$T > T_3 + l_c + a_{\mathrm{eff}}, \tag{27}$$

where $T_1 = T_2 = T$. The cavity losses must be less than M_1 and M_2 mirror transmissions to maintain a good impedance match. From Eq. (27), a cavity with high finesse (small T) is more susceptible to frequency-degenerate mode coupling than a low-finesse cavity. Thus, modal frequency degeneracy significantly affects resonator coupling efficiency with important consequences for circulating fundamental-mode power and gravitational-wave detection as will be discussed in subsequent sections.

3. Thermal Loading Experiment

Figure 3 shows the schematic of the experimental layout for testing the thermal response of a modecleaner. A finesse-of-50 "filter modecleaner" cleans a 30 W Nd:YAG master oscillator power amplifier (MOPA) laser beam by transmitting a spatially filtered fundamental mode with no discernible higher-order modal content. Low-loss optics for mode-matching and beam steering of the filtered laser beam keep thermal effects from these optics below a level that would impact the experiment. The filtered fundamental mode is subsequently mode-matched into the modecleaner to be tested under thermal load, known as the "modecleaner under test." Either the absorbing modecleaner or the low-loss modecleaner serve as the modecleaner under test. The filter modecleaner and modecleaner under test are locked to resonance using the Pound–Drever–Hall technique. The transmitted beam is then analyzed for higher-order modes with a "mode analyzer." The mode analyzer's length is linearly scanned using the PZT attached to mirror M_3 to measure the fundamental-mode power coupled into the cavity. Any higher-order modes in this beam are also measured with the same cavity scan. The transmission of the modecleaner under test is also analyzed for power variation through a data acquisition system. The filter modecleaner, modecleaner under test, and mode analyzer are identical in geometry with a perimeter of 42 cm and an M_3 radius of curvature of 1 m. Table 1 lists the relevant parameters of each cavity.

A modecleaner is tested under different conditions depending on the polarization of the incident light. A net π phase shift between the s and p polarizations results from the odd number of intracavity reflections in a modecleaner. Thus, the resonances of the two polarizations do not overlap in frequency. This

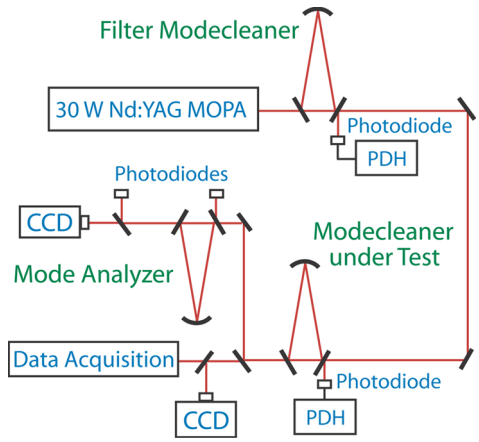

Fig. 3. (Color online) Experimental layout for testing a ring resonator (modecleaner) under thermal load. The filter modecleaner with a finesse of 50 filters the incident 30 W Nd:YAG master oscillator power amplifier (MOPA) laser beam to provide a spatially filtered, fundamental-mode input beam to illuminate the modecleaner under test. Output from the modecleaner under test is incident on the mode analyzer and data acquisition system for modal analysis and transmission monitoring. All cavities are locked to resonance using the Pound–Drever–Hall (PDH) technique.

allows a modecleaner to be locked to one polarization with excellent rejection of the orthogonal polarization [16]. Each polarization state also has a different reflectivity for M_1 and M_2 and, hence, a different finesse. This allows a modecleaner to be thermally loaded with differing levels of input power depending on the intracavity power enhancement of a given input polarization, as listed in Table 1.

A. Measurements of Accidental Modal Frequency Degeneracy Induced by Thermal Loading in the Absorbing Modecleaner

1. *p* Polarized Cavity

The absorbing modecleaner is illuminated with *p* polarized light and locked on resonance with the Pound–Drever–Hall technique. Incident power is increased in steps and the cavity relocked at each power increment. The absorbing modecleaner's transmitted beam is scanned in the mode-analyzer cavity, giving a measure of the fraction of fundamental-mode power contained in the beam relative to the total power. Figure 4 plots the transmitted fundamental-mode power fraction as a function of absorbed power for incident power up to 6 W. As shown in Table 1, the input power is enhanced by a factor of 105 inside the *p* polarized cavity.

As shown in Fig. 4, the fundamental-mode content decreases rapidly beyond 40 mW of absorbed power but also dips at specific absorbed powers. The first dip in fundamental-mode transmission occurs at 9 mW of absorbed power, resulting in a 1% drop in transmitted fundamental-mode power. A 7% dip occurs at 35 mW of absorbed power. Power coupled to the LG_{23} and $TEM_{11,0}$ modes at 9 mW and 35 mW, respectively, dominates these degradations of the transmitted beam. From Eq. (25), a_{eff} is calculated from the additional round-trip loss needed to produce the observed dips in fundamental-mode power. Values of a_{eff} for LG_{23} and $TEM_{11,0}$ are 82 and 530 ppm, as shown in Table 2. At absorption levels where specific higher-order mode coupling is not observed, a maximum of 2% of power is coupled into the TEM_{20} and TEM_{02} modes from the change in cavity eigenmode beam radius compared to the incident beam radius. Other higher-order modes are also resolved by the mode analyzer at these absorption levels but contain an insignificant amount of power. For example, the LG_{13} and LG_{33} modes are also measured with the mode analyzer at 9 mW of absorption

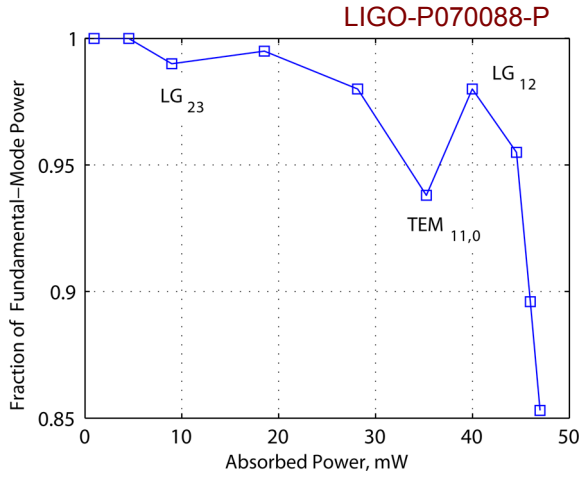

Fig. 4. (Color online) Fraction of transmitted fundamental-mode power relative to total transmitted power of the absorbing modecleaner locked to resonance in *p* polarization versus absorbed power. Power enhancement in *p* polarization is 105 with a maximum input power of 6 W. Beyond 40 mW of absorbed power, the fraction of fundamental-mode power in the absorbing modecleaner's transmitted beam rolls off sharply from coupling to the frequency-degenerate the LG_{12} mode. Fundamental-mode power coupling to the frequency-degenerate LG_{23} and $TEM_{11,0}$ modes occurs at 9 mW and 35 mW of absorbed power, respectively.

but contain a negligible amount of power. At 35 mW of absorbed power, a small amount of power couples to the $TEM_{13,0}$ and TEM_{90} modes in addition to the $TEM_{11,0}$ mode.

Figure 5(a) shows a CCD-camera image of the $TEM_{11,0}$ mode that overlaps in frequency with the fundamental mode of the absorbing modecleaner at 35 mW of absorbed power. Figure 5(b) shows the same $TEM_{11,0}$ mode after filtering through the mode analyzer. The highly distorted transmitted beam at 47 mW of absorbed power is shown in Fig. 5(c). Figure 5(d) clearly demonstrates, using the mode analyzer, that the overlapping mode is LG_{12}.

Figure 6 shows the absorbing modecleaner's transmitted power no longer increases linearly with input power as the frequency-degenerate LG_{12} mode strongly couples power from the fundamental mode beyond 40 mW of absorbed power (5 W of input power). a_{eff} from power coupled to LG_{12} is estimated at 1390 ppm. Coupling to other higher-order modes is minimal; the measured LG_{22} mode contains 17× less power than the LG_{12} mode.

Figure 7 shows the absorbing modecleaner's transmitted and reflected power fluctuating as a function of time for 47 mW of absorbed power (6 W incident

Table 1. Properties of Modecleaners for Thermal Loading Experiment: Polarization Dependence, Absorption and Power Enhancement

	Filter Modecleaner	Absorbing Modecleaner	Low-Loss Modecleaner	Mode-Analyzer Modecleaner
Absorption	<3.8 ppm	81 ppm	3 ppm	3 ppm
p Polarization Finesse	50	330	330	330
s Polarization Finesse	NA	5500	5500	5500
p Polarizatin Enhancement[a]	16	105	105	105
s Polarization Enhancement[a]	NA	1200	1200	1200

[a]Power enchancement is defined by Eq. (9).

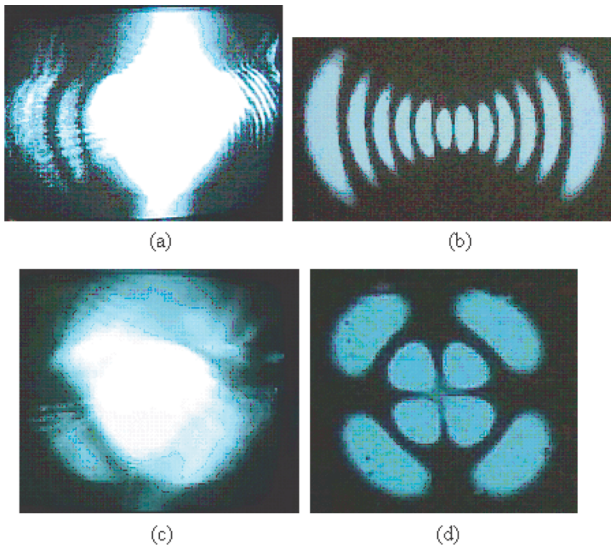

Fig. 5. (Color online) (a) The CCD image shows that the transmitted beam of the absorbing modecleaner contains both TEM_{00} and $TEM_{11,0}$ modes at 35 mW of absorbed power. The CCD camera is allowed to be slightly saturated to fully resolve the higher-order mode. (b) Image shows the $TEM_{11,0}$ mode when the beam from image (a) is filtered with the mode analyzer. (c) and (d) Images show the absorbing modecleaner's transmitted beam and resultant filtering via the mode analyzer at 47 mW of absorbed power, respectively, clearly showing the higher-order mode is LG_{12}.

power). At 47 mW of absorption and beyond, steady, locked transmitted power from the absorbing modecleaner is no longer achieved. A thermally-dependent, periodic-power fluctuation causes the transmitted power to vary by as much as 75% at frequencies ranging from 14 to 30 Hz. The fluctuation depth increases with absorption, while the frequency decreases until the servo can no longer maintain lock with the large power variation. During one thermal cycle, the transmitted mode morphs from the fundamental mode to LG_{12}, indicating that significant power is coupled into the LG_{12} mode. For a symmetric thermal deformation, coupling between the fundamental mode and LG_{12} is zero, as given by Eq. (23). A slight asymmetry stemming from optic imperfections or tilt must be present in the absorbing modecleaner to allow coupling between these modes. Increasing a_{eff} from power coupling to LG_{12} violates the condition given by Eq. (27) for a nearly impedance-matched modecleaner. This causes a rapid decline in power coupled into the cavity as seen from the increase in reflected power during one cycle. The corresponding decrease in transmitted power, and hence intracavity power, allows the absorbing mirror M_3 to cool slightly on a thermal time scale. a_{eff} decreases as M_3 cools from the decline in thermal load, thus allowing the cycle to repeat as power again builds up in the fundamental mode. The authors are currently developing a model for this phenomenon. The onset of this thermally-induced variation in transmission represents a thermal limit of the circulating fundamental-mode power of a resonant cavity.

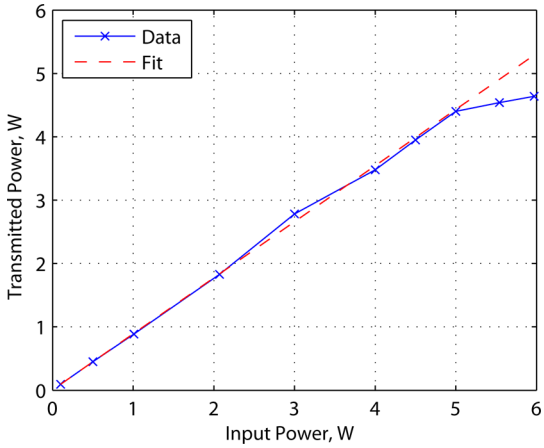

Fig. 6. (Color online) Transmitted power versus input power for the absorbing modecleaner. Beyond 40 mW of absorbed power (5 W of input power), strong coupling from the fundamental mode to the frequency-degenerate LG_{12} mode causes the transmitted power to no longer increase linearly with input power.

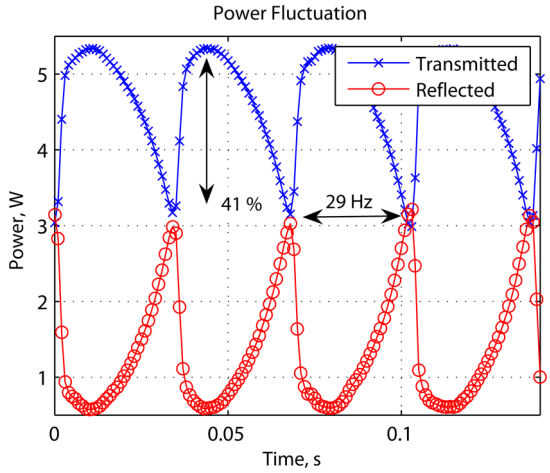

Fig. 7. (Color online) Periodic fluctuation in the transmitted and the reflected power from the absorbing modecleaner at 6 W of incident power. For 47 mW of absorbed power, the transmission of the absorbing modecleaner fluctuates at a frequency of 29 Hz with a fluctuation depth of 41%.

Figure 8 shows $g_1 g_2$ as a function of absorbed power for the modecleaner. The predicted modal frequency overlaps versus absorbed power with indicated mode-index sums defined by Eqs. (5) and (6) are highlighted on the graph. Higher-order modal frequency overlap with the fundamental mode is used to estimate the thermal distortion of a cavity's mirrors. When a higher-order mode overlaps in frequency with the fundamental mode, the new hot-cavity g-factor product can be deduced. The particular mode observed experimentally for a given mode-index sum may be governed by numerous factors such as astigmatism, scatter, and optic imperfections. For example, using Eq. (22), the qth axial LG_{12} mode with mode-index sum of four overlaps with the $(q\text{th} - 1)$ axial fundamental mode when a modecleaner's g-factor product is equal to 0.8536. From this new g-factor product, the hot radius of curvature of the absorbing modecleaner's curved mirror is cal-

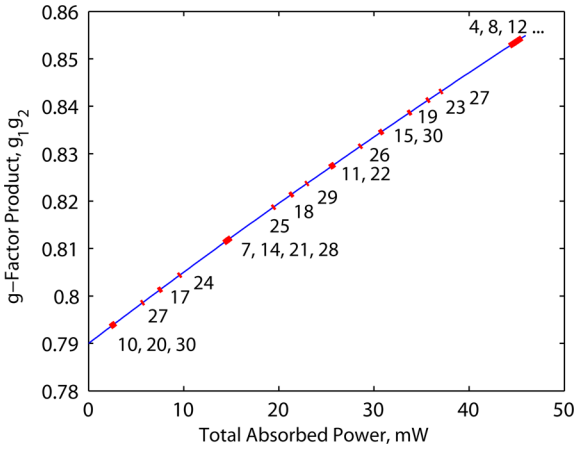

Fig. 8. (Color online) Absorbing modecleaner's g-factor product versus absorbed power. Predicted mode overlaps are highlighted along the curve with the appropriate mode-index sums [defined as $m+n$ for TEM_{mn} modes and $2p+l$ for LG_{pl} modes satisfying Eqs. (21) and (22)]. This plot applies for both p and s polarization, where the intracavity power enhancement is 105 and 1200, respectively. The range of each overlap is estimated from the change in the g-factor product needed for a higher-order mode to overlap within the modecleaner's undistorted full width at half-maximum (FWHM) linewidth.

culated to be 1.43 m, implying a 40% change in curvature from the undistorted curvature of 1 m. A calculation of the absorbed power from this new radius of curvature gives an absorption of 45 mW, which agrees with the measured 44–47 mW range of absorbed power where the LG_{12} mode is observed. The maximum curvature change of 40% implies the size of the cavity fundamental-mode waist increases by 7%. This change in eigenmode size alters the overlap between the intracavity fundamental and input fundamental mode from Eq. (24) by about 1% [15,17]. Thus, coupling to a frequency-degenerate higher-
order mode can degrade beam quality prior to any significant thermally-induced change in the waist size of the cavity's fundamental mode.

Table 2 summarizes the calculated and measured absorption from the observed frequency-degenerate higher-order modes and the calculated, thermally distorted radius of curvature of M_3. Disagreements between calculated and measured absorption may arise from a thermally-dependent resonance-frequency shift. An *et al.* [18] have shown that a change in the cavity length from thermal expansion

Table 2. Calculated and Measured Absorbed Power in the Absorbing Modecleaner for Three Observed Higher-Order Modes and Calculated Hot Radius of Curvature (ROC)

Observed Mode	LG_{23}	$\mathrm{TEM}_{11,0}$	LG_{12}
Calculated Absorption (mW)	14.6	25.6	45
Measured Absorption (mW)	9	35	44–47[a]
M_3 Hot ROC (m)	1.11	1.22	1.43
a_{eff} (ppm)	82	530	1390

[a] LG_{12} mode is observed over a range of absorbed powers.

of optics may lead to a shift in the resonance frequency proportional to the intracavity power. Thus, the power-induced resonance frequency shift leads to a broader range of frequency degeneracy between a higher-order and fundamental mode. This thermally-dependent frequency shift gives an estimated 8× broader frequency range of overlap compared to the cold-cavity linewidth when coupling to the LG_{12} mode is observed. For example, 1 mW of absorbed power moves the LG_{12} mode across the cold-cavity linewidth. The thermally-dependent frequency shift increases this range to 8 mW. Another source of disagreement between measured and calculated absorption occurs from the assumption that the higher-order modal resonance frequency overlaps with the fundamental-mode frequency at maximum resonance. In reality, the higher-order modal frequency falls somewhere within the cavity linewidth. The overlap within the cavity linewidth together with the thermally-dependent frequency shift can give a large range of absorbed power over which modal frequency degeneracy may occur.

2. *s* Polarized Cavity

Modal frequency degeneracy is much stronger for locking the absorbing modecleaner to resonance in high finesse with s polarized light and occurs at a lower absorption threshold than in the p polarized, low-finesse case. From Eq. (9) and Table 1, the intracavity power enhancement for s polarization is 1200, while for p polarization it is 105. For higher finesse, M_1 and M_2 transmission for s polarized light is less than the transmission for p polarized light. As a result, smaller values of a_{eff} break the impedance-matching condition given in Eq. (27).

Figure 8 is also applicable to frequency-degenerate higher-order modes observed in s polarization. The first observed modal frequency degeneracy couples 4% of fundamental-mode power to a $\mathrm{TEM}_{9,21}$ mode at 4.25 mW of absorbed power. This degeneracy gives $a_{\mathrm{eff}} = 56$ ppm. From Fig. 8, observing a mode with index-sum of 30 is plausible since the absorption threshold for coupling to these modes is predicted to be near 2.5 mW. The modecleaner aperture diameter is 13× larger than the beam diameter, resulting in low diffraction loss for large-diameter higher-order modes. As the thermal load is increased, strong coupling to multiple frequency-degenerate higher-order modes rapidly degrades the fundamental-mode transmission with fractional fundamental-mode power dropping to as low as 57% at 12 mW of absorbed power (300 mW of incident power), giving a_{eff} a value of 540 ppm.

Figure 9 shows a close-up of the power spectrum measured by the mode analyzer when scanned with the absorbing modecleaner's transmitted beam at 10 mW of absorbed power (200 mW of incident power). Power transfer to multiple frequency-degenerate higher-order modes is apparent with strong coupling to one mode spaced closely to the fundamental mode.

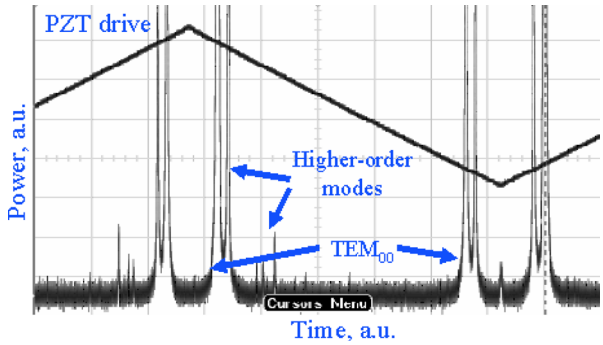

Fig. 9. (Color online) A close-up of an oscilloscope trace of the transmitted power spectrum from the mode analyzer when scanned with the absorbing modecleaner's transmitted beam at 10 mW of absorbed power (200 mW input power) in *s* polarization. The triangle wave shows the PZT drive signal for the mode analyzer. Coupling to multiple higher-order modes is visible with strong coupling to the LG_{15} mode, which is closely spaced to the fundamental mode.

This strongly coupled higher-order mode is LG_{15}. In Fig. 8, this mode has a predicted overlap absorption of 14 mW from its mode-index sum of 7 [Eq. ((5)]. Observing modal frequency degeneracy with LG_{15} at an absorbed power of 10 mW is in reasonable agreement with the predicted absorption of 14 mW. Strong coupling to frequency-degenerate higher-order modes is explained by the higher finesse for *s* than for *p* polarization. Any higher-order mode degenerate in frequency with the fundamental mode sees a power enhancement nearly 12× larger for *s* versus *p* polarization in a modecleaner. The thermally-dependent shift in frequency from thermal expansion of cavity optics described in Section 3.A.1 also plays a role in the overlap of higher-order modes with the fundamental mode [18]. For example, the resonant frequency shift at 12 mW of absorbed power causes the frequency overlap range of degenerate higher-order modes to increase by a factor of 25 when compared to the cold-cavity linewidth. The thermally-dependent frequency shift is proportional to finesse, resulting in a larger frequency shift for higher finesse.

B. Measurements of Accidental Frequency Degeneracy in the Low-Loss Modecleaner

Thermally loading the low-loss modecleaner in *s* polarization with a power enhancement of 1200 shows that modal frequency degeneracy is not limited to the characteristics of the absorbing modecleaner but applies to all cavities with similar characteristics. The low-loss modecleaner has a 3 ppm absorption loss distributed equally among the mirror coatings. Predictions of modal frequency degeneracy as a function of absorbed power are modeled as in Section 2, but thermal deformation of mirrors M_1 and M_2 are included. Transmission increases linearly with input power up to 8 W where 20 mW of absorbed power is reached in the cavity. Power transfer to frequency-degenerate higher-order modes rapidly degrades the beam quality beyond 20 mW of absorbed power. Frequency-degenerate higher-order modes are also observed at absorptions well below the maximum. The first overlap occurs at 5.1 mW of absorbed power with another at 10 mW. The large number of nodes in the higher-order modes observed at these absorbed powers make their identification difficult. The $TEM_{0,27}$ and $TEM_{17,0}$ modes are frequency-degenerate for 7.1 mW and 9.4 mW of absorption, respectively. These frequency degeneracies are calculated from Eqs. (21) and (22) for the low-loss modecleaner and match well with those observed in the experiment. For *p* polarized input, the low-loss modecleaner begins to show some power coupling to higher-order modes at 5.1 mW of absorbed power, which is limited by maximum available input power. From these results, accidental frequency degeneracies may occur and are predictable for any resonator configuration if the losses are known.

4. Predictions for Future LIGO Resonators

In this section, modal frequency degeneracy is predicted for resonators in future LIGO interferometers. Resonators that undergo significant thermoelastic deformation from coating absorption include the modecleaners and Fabry–Pérot light-storage arm cavities for Enhanced and Advanced LIGO. Since a weak gravitational-wave signal is detected via the resonant fundamental mode of the arm cavities, frequency degeneracy caused by thermal loading impacts interferometer performance. To predict the occurrence of frequency-degenerate higher-order modes, new, hot-cavity g-factors are calculated for the maximum thermal load in a given cavity. The new g-factor product is utilized in Eqs. (21) and (22) to find higher-order modes that are frequency-degenerate with the fundamental mode. The coating absorption is assumed to be the same for all resonator mirrors.

A. Modecleaners for Enhanced and Advanced LIGO

Modecleaners are employed in two locations for filtering the input laser beam to the interferometer. A table-top modecleaner identical in geometry to the modecleaners used in the thermal loading experiment provides the initial spatial-mode filtering of the high-power laser. A modecleaner with a perimeter of several tens of meters and suspended mirrors (suspended modecleaner) provides additional spatial and temporal filtering of the laser beam incident on the interferometer [19]. These modecleaners utilize mirrors with low-loss coatings on fused silica substrates. While the thermal conductivity of fused silica is low, its small thermal expansion coefficient, uniformity, and ease of manufacture in large diameter make it a desirable substrate material for LIGO.

Enhanced and Advanced LIGO table-top modecleaners filter the 35 and 200 W proposed laser systems, respectively. The table-top modecleaner for Enhanced LIGO has a finesse of 200, while a modecleaner with finesse of 50 is used for Advanced LIGO. Coating absorptions of 6 and 8.5 ppm for the Enhanced and Advanced LIGO table-top modecleaners, respectively, lead to the first accidental frequency de-

generacies that have mode-index sums of 10, 20, and 30. For a proposed coating absorption loss of 1 ppm, the table-top modecleaners for Enhanced and Advanced LIGO will not experience higher-order modal frequency degeneracy at the proposed incident power levels.

However, the suspended modecleaners for Enhanced and Advanced LIGO experience modal frequency degeneracy for 1 ppm of coating absorption. Table 3 lists the properties of the suspended modecleaners, as well as their frequency-degenerate mode-index sums. The frequency-degenerate higher-order modes have large order (mode-index sum of 11 and higher), suggesting that a proper choice of aperture may suppress power coupling to these modes. The aperture formed by the mirror itself compared with the beam size is insufficient to suppress higher-order modes. If coating absorptions for each Enhanced and Advanced LIGO suspended modecleaner reach 4.7 and 4.2 ppm, respectively, a frequency-degenerate mode-index sum less than 10 is attained. Thus, with coating absorptions at 1 ppm or less and proper aperturing, higher-order mode coupling is avoidable in the suspended modecleaners at the proposed operating power levels.

B. Fabry–Pérot Arm Cavities for Enhanced and Advanced LIGO

LIGO has 4 km Fabry–Pérot cavities in each arm of its Michelson configuration to increase interaction time with a gravitational wave [4]. These resonators experience the highest circulating power of any cavity employed in LIGO. For 25 W of incident power on the interferometer for Enhanced LIGO, the arm cavities experience a maximum circulating power of 100 kW [20]. For Advanced LIGO with 125 W of incident power on the interferometer, the arm cavities will be subjected to 800 kW of circulating power [21]. Table 4 gives a list of arm-cavity parameters.

Figure 10 shows $g_1 g_2$ versus the coating absorption of a single mirror for the Enhanced LIGO long-radius arm cavities. Mode-index sums for frequency-degenerate higher-order modes are marked along the graph. Vertical lines denote the maximum absorbed power experienced for a given coating absorption at 100 kW of circulating power. Diffraction loss also plays a roll in the higher-order modes an arm cavity may support. The maximum mode-index sum supported by a resonator is approximated by $s_{\max} \approx (a/w)^2$, where a and w are the mirror and beam radii, respectively [9]. $s_{\max} \approx 8$ for Enhanced LIGO. From Fig. 10, an Enhanced LIGO arm cavity with 100 kW of circulating power is likely to show modal frequency degeneracy at 800 mW of total coating absorption for a mode-index sum of 7. To avoid this modal frequency overlap, a mirror's coating absorption should be less than 3.8 ppm, demonstrating that low coating absorption during extended operation is important for minimizing higher-order modal frequency degeneracy.

Figure 11 shows accidental modal frequency degeneracy occurring in an Advanced LIGO near-spherical arm cavity with modes having index sums less than 8 at 706 mW, 1.76 W, and 3.48 W total coating absorption for mode-index sums of 7, 6, and 5, respectively, at 800 kW of circulating power. The maximum supported mode-index sum, $s_{\max} \approx 8$, is the same as that for Enhanced LIGO. Since an Advanced LIGO arm cavity approaches a confocal resonator as it is heated, its g-factor product decreases until the mirror radii of curvature is equal to the length of the cavity. This arm cavity is unlikely to become confocal via thermal loading since the mirror radii of curvature must change by nearly a factor of 2. The cold Advanced LIGO arm cavity needs only 14 mW of total coating absorption to reach accidental frequency degeneracy at a mode-index sum of 8, making this overlap unavoidable as power is increased. A coating absorption of less than 0.44 ppm must be maintained during extended operation to avoid the frequency-degenerate modes at a mode-index sum of 7. Achieving uniform 0.44 ppm coating absorption may be difficult given the limits of available dielectric-coating technology. Furthermore, coating inhomogeneities from dust or other contamination may also induce modal frequency degeneracy at thresholds lower than those predicted for uniform coating absorption. Coating uniformity will be most critical for the arm cavities of Advanced LIGO.

Table 3. Enhanced and Advanced LIGO Suspended Modecleaner Properties and Frequency-Degenerate Higher-Order Modes for 1 ppm Coating Absorption Loss

Suspended Modecleaner	Enhanced LIGO	Advanced LIGO
Perimeter (m)	24.48	33.33
M_3 Radius of Curvature (m)	17.25	25.95
Finesse	1700	500
Maximum Circulating Power (kW)	15	24
Total Coating Absorption [a](mW)	23.5	11.5/60
Degenerate Mode-Index Sums	11 and 22	22/17

[a]Single-optic coating absorption ×3.

Table 4. Enhanced and Advanced LIGO Fabry–Pérot Arm Cavity Properties

	Enhanced LIGO[a]	Advanced LIGO[b]
Radius of Curvature (m), M_1	13910	2076
Radius of Curvature (m), M_2	7260	2076
Cavity Length (m)	3995	3995
Optic Radius (cm)	12.5	17
Beam Radius at M_1 (cm)	3.61	5.96
Beam Radius at M_2 (cm)	4.55	5.96
Finesse	220	1257
Maximum Circulating Power (kW)	100	800

[a]Enhanced LIGO arm cavity properties are from the LIGO site in Hanford, Wash.

[b]Advanced LIGO data are based on the latest design information [21].

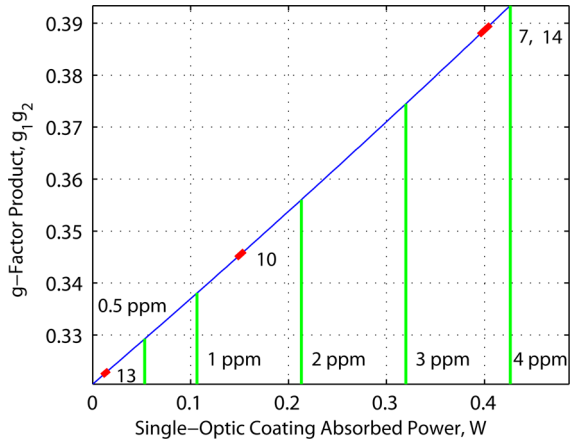

Fig. 10. (Color online) Enhanced LIGO arm-cavity g-factor product versus single-optic coating absorbed power for 100 kW of circulating power. Predicted mode-index sums giving higher-order modal frequency degeneracy are highlighted along the curve similar to that shown in Fig. 8. Vertical lines mark the maximum absorbed power at 100 kW for the specified coating absorption. The greater the absorption, the larger the number of possible frequency-degenerate higher-order modes.

5. Conclusion

We have shown that thermoelastic deformation from absorbed power in a mirror induces accidental frequency degeneracy of higher-order modes with the fundamental mode of a resonator. Experiments using a modecleaner with calibrated absorption loss demonstrated agreement between predicted and measured higher-order modal frequency degeneracies for a given absorbed power. Circulating power also governed the strength of the higher-order mode power coupling, resulting in greater coupling for higher finesse. Studies with a thermally loaded low-loss modecleaner showed that modal frequency degeneracy predictions are valid for any resonator configuration with knowledge of absorption loss and mirror thermal properties.

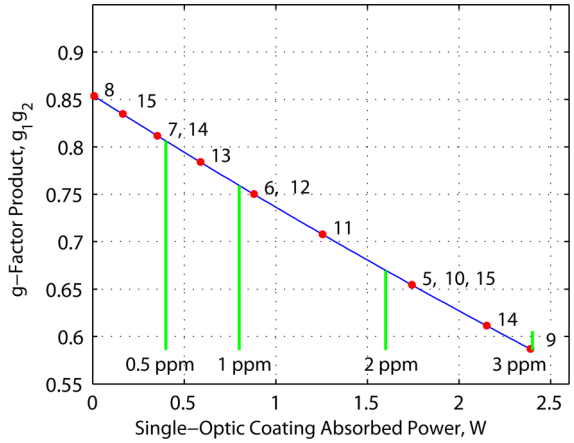

Fig. 11. (Color online) Advanced LIGO arm-cavity g-factor product versus single-optic coating absorbed power for 800 kW of circulating power. Predicted degenerate mode-index sums are indicated with dots on the graph and vertical lines mark the maximum absorbed power at 800 kW for the specified coating absorption. Advanced LIGO arm cavities become more susceptible to modal frequency degeneracy at low coating absorption because of high circulating power.

Based on modeling of the thermally-induced frequency degeneracies observed experimentally, frequency-degenerate modal predictions were made for future upgrades to LIGO. Suspended modecleaners for Enhanced and Advanced LIGO may avoid modal frequency degeneracy with proper aperturing and coating absorption of 1 ppm or less. While aperture size may suppress some higher-order modes in the arm cavities, modal frequency degeneracy is predicted in Enhanced LIGO for coating absorption exceeding 3.8 ppm and in Advanced LIGO for absorption greater than 0.44 ppm. These coating absorptions must be uniform across the mirror diameter and be maintained for extended operation of LIGO.

An interferometer that employs an all-reflective topology may use substrates with better thermal properties (e.g., silicon) than those only available for transmission at the operating wavelength of 1064 nm [22]. For example, the ratio of change in sagitta, δs, of fused silica to silicon is 20, implying that 20× the power may be absorbed in a silicon substrate than a fused silica one for the same thermoelastic deformation. An all-reflective Sagnac interferometer for gravitational-wave detection has been demonstrated using silicon optics [23]. Furthermore, silicon may be cooled to cryogenic temperatures where its thermal expansion coefficient approaches zero at 18 and 120 K [24], helping to avoid any thermally-induced modal frequency degeneracy. Alternative substrates and interferometer topology may be necessary to avoid thermal effects when considering gravitational-wave detectors beyond Advanced LIGO.

This work was supported by the National Science Foundation under grant PHY-05-02641. The authors thank members of the LIGO Scientific Collaboration for insightful discussion. A. Bullington also acknowledges support from a National Science Foundation Graduate Research Fellowship. Jerome Degallaix and Eric Gustafson provided valuable suggestions for the development of this work.

References

1. T. Kimura and K. Otsuka, "Thermal effects of a continuously pumped Nd^{3+}:YAG laser," IEEE J. Quantum Electron. **7**, 403–407 (1971).
2. T. Kimura, K. Otsuka, and M. Saruwatari, "Spatial hole-burning effects in a Nd^{3+}:YAG laser," IEEE J. Quantum Electron. **7**, 225–230 (1971).
3. T. Klaassen, J. de Jong, M. van Exter, and J. P. Woerdman, "Transverse mode coupling in an optical resonator," Opt. Lett. **30**, 1959–1961 (2005).
4. P. Fritschel, "The second generation LIGO interferometers," in *Proceedings of Astrophysical Sources for Ground-Based Gravitational Wave Detectors*, J. M. Centrella, ed. (American Institute of Physics, 2001), pp. 15–23.
5. R. Adhikari, P. Fritschel, and S. Waldman, "Enhanced LIGO," http://www.ligo.caltech.edu/docs/T/T060156-01.pdf.

6. E. D'Ambrosio, LIGO Laboratory, California Institute of Technology, MS 18-34, Pasadena, CA 91125, USA, and A. M. Gretarsson, V. Frolov, B. O'Reilly, and P. K. Fritschel, are preparing a manuscript to be called "Effects of mode degeneracy in the LIGO Livingston Observatory recycling cavity."
7. V. Loriette and C. Boccara, "Absorption of low-loss optical materials measured at 1064 nm by a position-modulated collinear photothermal detection technique," Appl. Opt. **42**, 649–656 (2003).
8. C. Janke, "Thermal loading of optical components in interferometric systems," presented at the LIGO Scientific Collaboration Conference, Baton Rouge, Louisiana, (March 2001).
9. A. E. Siegman, *Lasers* (University Science, 1986). Errata URL: http://www.stanford.edu/siegman/lasers_book_errata.pdf.
10. R. W. P. Drever, J. L. Hall, F. V. Kowalski, J. Hough, G. M. Ford, A. J. Munley, and H. Ward, "Laser phase and frequency stabilization using an optical resonator," Appl. Phys. B, Laser Opt. **31**, 97–105 (1983).
11. W. Winkler, K. Danzmann, A. Rudiger, and R. Schilling, "Heating by optical absorption and the performance of interferometric gravitational-wave detectors," Phys. Rev. A **44**, 7022–7036 (1991).
12. N. Uehara and K. Ueda, "Accurate measurement of the radius of curvature of a concave mirror and the power dependence in a high-finesse Fabry–Pérot interferometer," Appl. Opt. **34**, 5611–5619 (1995).
13. R. Paschotta, "Beam quality deterioration of lasers caused by intracavity beam distortions," Opt. Express **14**, 6069–6074 (2006).
14. P. T. Beyersdorf, S. Zappe, M. M. Fejer, and M. Burkhardt, "Cavity with a deformable mirror for tailoring the shape of the eigenmode," Appl. Opt. **45**, 6723–6728 (2006).
15. H. Kogelnik, "Coupling and conversion coefficients for optical modes," in *Proceedings of the Symposium on Quasi-Optics*, (Polytechnic Press, 1964), pp. 333–347.
16. S. Saraf, R. L. Byer, and P. J. King, "High-extinction-ratio resonant cavity polarizer for quantum-optics measurements," Appl. Opt. **46**, 3850–3855 (2007).
17. N. Uehara, E. K. Gustafson, M. M. Fejer, and R. L. Byer, "Modeling of efficient mode matching and thermal-lensing effect on a laser-beam coupling into a mode-cleaner cavity," Proc. SPIE **2989**, 57–68 (1997).
18. K. An, B. A. Sones, C. Fang-Yen, R. R. Dasari, and M. S. Feld, "Optical bistability induced by mirror absorption: measurement of absorption coefficients at the sub-ppm level," Opt. Lett. **22**, 1433–1435 (1997).
19. D. Tanner, Department of Physics, University of Florida, P.O. Box 118440, Gainesville, Florida, 32611 (personal communication, 2007).
20. R. Adhikari, Department of Physics, California Institute of Technology, Physics Department 103-33, Pasadena, California, 91125 (personal communication, 2007).
21. P. Fritschel, "Advanced LIGO interferometer parameters," http://emvogil3.mit.edu/∼pf/advligo/SYS/ALparameters.htm.
22. K. X. Sun and R. L. Byer, "All-reflective Michelson, Sagnac, and Fabry–Pérot interferometers based on grating beam splitters," Opt. Lett. **23**, 567–569 (1998).
23. P. T. Beyersdorf, R. L. Byer, and M. M. Fejer, "Results from the Stanford 10 m Sagnac interferometer," Class. Quantum Grav. **19**, 1585–1589 (2002).
24. S. Rowan, J. Hough, and D. R. M. Crooks, "Thermal noise and material issues for gravitational wave detectors," Phys. Lett. A **347**, 25–32 (2005).